

How Laser Diode (LD) Intensity Modulation Induced by Current Tuning Affects the Performance of an Open-loop Resonator Fibre Optic Gyro (R-FOG) with Sinusoidal Wave Modulation

D. YING*, Q. LI, H. MA AND Z. JIN

*Micro-Satellite Research Centre, Zhejiang University, 38 Zheda Road,
Hangzhou City 310027, China*

We present how the laser diode (LD) current tuning induced intensity modulation affects the performance of an open-loop resonator fibre optic gyro (R-FOG) with sinusoidal wave modulation. The expression for the demodulation curve under intensity modulation caused by the dynamic input rotation angular rate and varied environmental factors induced resonance frequency drift is provided. Numerical investigation shows that under the intensity modulation effect due to dynamic input rotation angular rate, which results in a bending trend for the linear part of demodulation curve, the linearity of R-FOG system is deteriorated, and the scale factor nonlinearity of gyro output increases as the frequency-intensity conversion coefficient of the LD increases. By simulating the demodulation curve with different amount of resonance frequency drift due to varied environmental factors, the slope of the linear part is found to fluctuate under the resonance frequency drift induced intensity modulation, and it causes the scale factor of the practical R-FOG system to fluctuates. This scale factor fluctuation results in a system measurement error, which is proven to increase as the amount of resonance frequency drift or input rotation angular rate increases, and numerical calculation result shows this large system error should be counted for an open-loop R-FOG system.

Keywords: Laser diode (LD), resonator fibre optic gyro (R-FOG), current modulation, intensity modulation, sinusoidal wave modulation, scale factor nonlinearity

*Corresponding author: Tel: +86 (0)571 8795 2587; Fax: +86 (0)571 8795 2587;
E-mail: dqying@zju.edu.cn

1 INTRODUCTION

The resonator fiber optic gyro (R-FOG) has potential to be used as a high accuracy inertial rotation sensor based on the Sagnac effect [1-5]. It has been theoretically proven that an R-FOG could achieve similar shot noise limited performance as an interferometric fiber optic gyro (I-FOG) but requires a shorter length of fiber [2], which is significant in reducing gyro's size and cost. Differing from the I-FOG, the R-FOG needs a highly coherent laser to achieve high finesse resonance [6]. In order to satisfy this requirement, Nd:YAG lasers, He-Ne lasers and fiber lasers have been chosen as the laser source to setup the R-FOG system [7-9]; however, these laser sources generally have large size that gets in the way of the miniaturization for the R-FOG system. Compared with the laser sources mentioned above, semiconductor lasers are more compact and has much smaller size [10]. And with the development of opto-electronic technology, highly coherent laser diodes (LD) instead of those lasers mentioned above have been applied in the R-FOG system to greatly minimize the size of the R-FOG system [11-14].

The frequency of the light wave emitted from the LD could be easily modulated by tuning the injection current directly [15-16]. And using this injection current tuning method, it could be realized to lock the laser central frequency to the resonance frequency of the fiber ring resonator (FRR) of an R-FOG system with the laser source of LD, which is a critical signal processing technique for accomplishing the rotation angular rate detection [14]; however, when the injection current of the LD is tuned, accompanying intensity modulation would also be induced, which affects the performance of the R-FOG system [17]. Through numerical simulation and experimental investigations, Ma *et al* [17, 18] and Lei *et al* [19, 20] have showed that the intensity modulation caused by the triangle wave current modulation would lead to the attenuation distortion of the resonance curve of the gyro; however, in-depth analysis of how the intensity modulation, especially caused by the dynamic input rotation angular rate and varied environmental factors induced resonance frequency drift, takes influence on the performance of the R-FOG with sinusoidal phase modulation has not been done. In R-FOG practical applications the resonance frequency of FRR is generally not fixed because it varies with the dynamic input rotation angular rate [4] and some environmental factors, such as temperature [2, 21]. As mentioned above, the frequency of the laser always tracks the varied resonance frequency in the R-FOG system, which is realized by tuning the injection current of the LDs; therefore, the resonance frequency fluctuation would lead to an intensity modulation, and finally exerts an influence on the performance of the R-FOG system.

This paper explores the effect of LD's accompanying intensity modulation on the performance of an open-loop R-FOG with sinusoidal phase modulation, and we focus here our analysis on the characteristics of the demodula-

tion curve affected by the dynamic input rotation angular rate and resonance frequency drift induced accompanying intensity modulation. We provide the expression for the demodulation curve under the LD's accompanying intensity modulation. By numerical simulation, how the accompanying intensity modulation due to the dynamic input rotation angular rate affects the demodulation curve and scale factor nonlinearity of the gyro output is discussed. Apart from that, how the resonance frequency drift induced intensity modulation affect the slope of the demodulation curve's linear part and the scale factor of the gyro system is studied, and the system measurement error due to this accompanying intensity modulation is calculated.

2 THEORETICAL FORMULATION

Figure 1 illustrates the system configuration of the open-loop R-FOG system with sinusoidal phase modulation [14, 22]. All the fibres are polarization preserving. The laser source employed in this system is LD. The central wavelength and linewidth of the LD is 1550 nm and 5 kHz, respectively. The laser is equally divided into two beams by coupler C0 and each beam is sinusoidal wave phase modulated by the LiNbO₃ phase modulators PM1 and PM2, respectively. And then, the two beams are injected into the FRR in the clockwise (CW) and counter clockwise (CCW) directions. The CW and CCW beams output from FRR are sensed by the InGaAs PIN photodetectors PD1 and PD2, respectively. The CCW signal is demodulated by the digital lock-in-amplifier LIA2, and then through the servo controller, the central frequency of the laser is locked to the CCW resonance of FRR by modulating the LD's injection current directly. The CW signal is demodulated by the

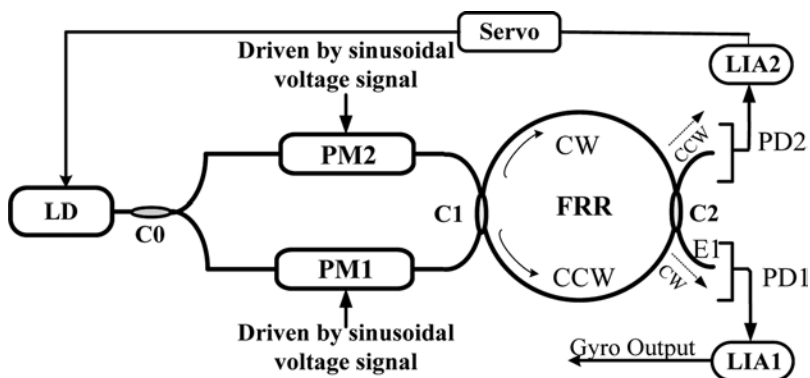


FIGURE 1

System configuration of the open-loop R-FOG with sinusoidal phase modulation. CW: clockwise; CCW: counter clockwise; LD: laser diode; C0-C2: couplers; PD1, PD2: photodetectors; PM1, PM2: phase modulators.

digital lock-in-amplifier LIA1 and the demodulated signal is proportional to the rotation rate [5].

The output electric field of the LD can be expressed as [23]

$$E_{LASER}(t) = E_0 \exp\left[j(2\pi f_0 t + \phi_0)\right] \quad (1)$$

where E_0 is the amplitude of the electric field of the laser light, f_0 is the central frequency of the laser and ϕ_0 is the initial phase. The laser's central frequency f_0 tracks the resonance frequency f_{R_CCW} of the FRR in CCW direction to make the operating point for the CCW beam always be fixed at the resonance [24]; therefore, Eq. (1) also can be written as

$$E_{LASER}(t) = E_0 \exp\left[j(2\pi f_{R_CCW} t + \phi_0)\right] \quad (2)$$

Using the Bessel function, the sinusoidal wave phase modulated electric field after PM1 can be written as [5, 25]

$$E_{M_CW}(t) = E_0 \sqrt{k_{C0}(1-\alpha_{C0})(1-\alpha_{PM1})} \sum_{n=-\infty}^{\infty} J_n(M) \exp\left[j(2\pi f_n t + \phi_0)\right] \quad (2)$$

where k_{C0} and α_{C0} are the intensity coupling coefficient and fractional intensity loss of coupler C0, respectively; α_{PM1} is the fractional insertion loss of PM1; M is phase modulation index, which is set as 2.405 rad in this paper for suppressing the carrier component [5, 26-28]; and $fn = f_{R_CCW} + nF_{CW}$, F_{CW} is the phase modulation frequency. Employing the field overlapping method [23, 29], the output field at E1 in Figure 1 can be written as

$$E_{O_CW}(t) = E_0 \sqrt{k_{C0}(1-\alpha_{C0})(1-\alpha_{PM1})} \sum_{n=-\infty}^{\infty} J_n(M) \exp\left[j(2\pi f_n t + \phi_0)\right] \cdot h_n \exp(j\phi_n) \quad (3)$$

where

$$h_n = QR \sqrt{\frac{1}{(1-TR^2)^2 + 4TR^2 \sin^2 \left[\frac{\pi(\Delta f_{RES} + nF_{CW})}{FSR} \right]}} \quad (4a)$$

$$\phi_n = -\frac{\pi f_n}{FSR} - \arctan \left\{ \frac{TR^2 \sin \left[2\pi \left(\frac{\Delta f_{RES} + nF_{CW}}{FSR} \right) \right]}{1-TR^2 \cos \left[2\pi \left(\frac{\Delta f_{RES} + nF_{CW}}{FSR} \right) \right]} \right\} \quad (4b)$$

and

$$T = \sqrt{1-k_{C1}} \sqrt{1-k_{C2}} \sqrt{1-\alpha_{C1}} \sqrt{1-\alpha_{C2}}, \quad (4c)$$

$$Q = \sqrt{k_{C1}k_{C2}} \sqrt{1-\alpha_{C1}} \sqrt{1-\alpha_{C2}}, R = \sqrt{1-\alpha_{L/2}}$$

where k_{C1} and k_{C2} are the intensity coupling coefficients of couplers C1 and C2, respectively; α_{C1} and α_{C2} are the fractional insertion loss of couplers C1 and C2, respectively; $\alpha_{L/2}$ is the fractional intensity loss for semi-loop of the FRR; $\Delta f_{RES} = f_{R_CCW} - f_{R_CW}$ is the resonance frequency difference between the CCW and CW propagating beams; f_{R_CW} is the resonance frequency of the FRR in CW direction; $FSR = c/(n_r L)$ is the free spectral range; L is the length of FRR; n_r is the refractive index of fiber and c is the light velocity in vacuum. Equation (4a) and Equation (4b) are the amplitude and phase of the FRR's transfer function in CW direction, respectively. According to Equation (4) the output signal of the photodetector PD1 can be written as

$$V_{PD_CW} = G_1 P_1 I \sum_{n=-\infty}^{\infty} \sum_{n'=-\infty}^{\infty} J_n(M) J_{n'}(M) \exp[j(n-n')2\pi F_{CW} t] \quad (5)$$

$$h_n h_{n'} \exp[j(\phi_n - \phi_{n'})]$$

where $G_1 = k_{C0}(1-\alpha_{C0})(1-\alpha_{PM1})$, P_1 is the photoelectric conversion coefficient of photodetector PD1 and I is the output intensity of LD. After demodulation with respect to the first harmonic, all the terms in Equation (5) are eliminated except those satisfying the condition $n' = n \pm 1$, then the demodulation signal output from LIA1 can be written as [25, 30]

$$V_{d_CW} = -G_1 P_1 A_{D1} I \sum_{n=-\infty}^{\infty} J_n J_{n+1} h_n h_{n+1} \sin(\phi_{n+1} - \phi_n) \quad (6)$$

where A_{D1} is the gain of lock-in-amplifier LIA1.

In the practical situation, the CCW resonance frequency f_{R_CCW} varies with resonance frequency difference Δf_{RES} proportional to input rotation angular rate and some environmental factors, such as temperature. Since the frequency of the LD always tracks the varied CCW resonance frequency f_{R_CCW} by tuning LD's injection current as mentioned above, the LD's output intensity, which is proportional to the injection current [17-20], would be modulated, and it would affect the characteristics of the gyro system. When this intensity modulation is considered, Equation (6) can be written as

$$V_{d_CW} = -G_1 P_1 A_{D1} \left(I_0 - k_i \frac{\Delta f_e}{k_f} - k_i \frac{\Delta f_{RES} / 2}{k_f} \right) \sum_{n=-\infty}^{\infty} J_n J_{n+1} h_n h_{n+1} \sin(\phi_{n+1} - \phi_n) \quad (7)$$

where Δf_e is the frequency drift of f_{R_CCW} due to environmental factors; $\Delta f_{RES}/2$ is the change of f_{R_CCW} because of the varied input rotation angular rate based on the Sagnac effect [4, 31]; k_f and k_i are respectively the frequency and intensity modulation coefficients of LD, and here we set $k = k_i/k_f$ as the frequency-intensity conversion coefficient; and I_0 is the LD's output intensity when the gyro is at rest. According to Equation (7) and the Sagnac effect [4, 31], the demodulation signal can be expressed as a function of input rotation angular rate by

$$V_{d_CW}(\Omega) = V_{d_CW} \left(\Delta f_{RES} = \frac{D\Omega}{n_r \lambda} \right) \quad (8)$$

where Ω is the rotation angular rate, D is the diameter of FRR, and λ is the central wavelength of laser. According to Equation (7) and Equation (8), it is found that both the resonance frequency drift and input rotation angular rate decides the demodulation signal, which would finally affect the performance of the gyro system.

3 SIMULATION AND DISCUSSION

Based on Equation (8) the numerical simulation on the performance of R-FOG under LD intensity modulation is carried out. Figure 2 shows the calculated demodulation curve near $\Omega = 0$ with $k = 0$, 3×10^{-4} , and

5×10^{-4} mW/Hz. In order to show the difference between the demodulation curves with and without intensity modulation more clearly, the values for k we set in this numerical simulation is much larger than the practical value of the LD we used in the system, which is actually in the order of 10^{-9} to 10^{-8} mW/Hz. Here, the environmental factors induced resonance frequency drift is firstly not considered for simplicity; therefore, Δf_e is fixed at 0, and in this case, the LD intensity modulation is only induced by the dynamic input rotation rate. The length, L , and diameter, D , of the FRR, respectively, are 12.00 and 0.14 m, the modulation frequency for CW loop is fixed at $FCW = 101$ kHz, the refractive index of the fiber nr is 1.455, all the fractional intensity loss α_{C0} , α_{C1} and α_{C2} for couplers C0, C1 and C2 respectively are 0.0228, the fractional insertion loss α_{PM1} of PM1 is 0.5, the intensity coupling coefficient k_{C0} of coupler C0 is 0.5, both the intensity coupling coefficients k_{C1} and k_{C2} for couplers C1 and C2 respectively are designed as 0.03, the fractional intensity loss α_{L2} for semi-loop of the FRR is 0.00035, the photoelectric conversion coefficient P_1 of PD1 is 0.5V/mW, the output intensity I_0 of LD is assumed to be 3 mW, and the gain A_{DI} of lock-in-amplifier LIA1 is 1. As can be seen in Figure 2, when the frequency-intensity conversion coefficient k is 0 that the LD intensity modulation is not considered, the demodulation curve is relatively straight and centrosymmetric; however, when the LD intensity modulation is considered that k is not 0, the demodulation curve gradually deviates from that without intensity modulation as the input rotation angular rate increases, and trends to be bent and non-centrosymmetric as shown in Figure 2. That would affect the linearity of the gyro system [27].

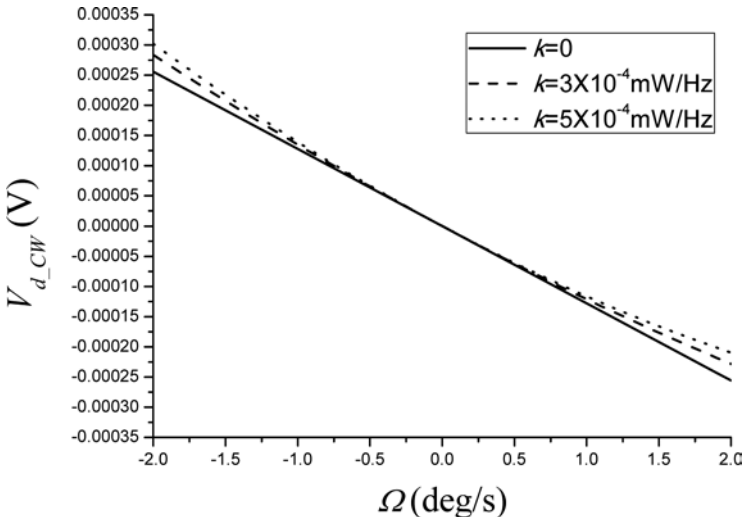


FIGURE 2
Demodulation curve with different values of k .

In order to further analyse how the intensity modulation affects the linearity of the gyro system, we use the least square method to fit the demodulation curve as [32-33]

$$\hat{V}_{d_CW} = K\Omega + F \quad (9)$$

where

$$K = \frac{\sum_{j=1}^N \Omega_{ij} \cdot V_j - \frac{1}{N} \sum_{j=1}^N \Omega_{ij} \cdot \sum_{j=1}^N V_j}{\sum_{j=1}^N \Omega_{ij}^2 - \frac{1}{N} \left(\sum_{j=1}^N \Omega_{ij} \right)^2} \quad (9a)$$

and

$$F = \frac{1}{N} \sum_{j=1}^N V_j - \frac{K}{N} \sum_{j=1}^N \Omega_{ij} \quad (9b)$$

where K is the scale factor, F is the fitting zero offset, Ω_{ij} is the j th input rotation angular rate, V_j is the gyro output corresponding to the j th input rotation angular rate Ω_{ij} , and N is the number of the input rotation angular rate. According to Equation (9), the scale factor nonlinearity could be calculated by [33]

$$K_n = \left| \frac{\hat{V}_{d_CW} - V_j}{|V_m|} \right|_{\max} \quad (10)$$

where $|V_m|$ is the maximum absolute value of the gyro output with maximum input rotation angular rate. According to Equation (9) and Equation (10), the theoretical scale factor nonlinearity could be predicted. Figure 3 shows the relationship between scale factor nonlinearity K_n and LD's frequency-intensity k . As can be seen in Figure 3, the scale factor nonlinearity K_n is only about 22.8 ppm in the ideal condition that $k = 0$. And as k increases, the scale factor nonlinearity also increases. Taking $k = 5 \times 10^{-9}$ mW/Hz as an example, the scale factor nonlinearity is increased to about 26.1 ppm, which would worsen the performance of the gyro system.

In addition to the dynamic input rotation angular rate, the environmental factors induced resonance frequency drift Δf_e also causes LD's intensity modulation. In order to discuss how this resonance frequency drift induced inten-

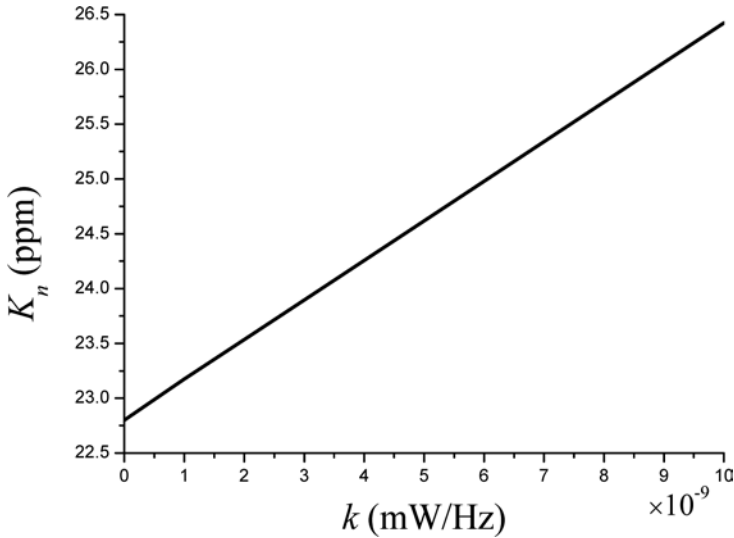


FIGURE 3

Graph showing the relationship between K_n and the value of k for the LD.

sity modulation affect the performance of the gyro system, we calculated the demodulation curve near $\Omega = 0$ with $\Delta f_e = 0$, $5FSR$, and $10FSR$ shown in Figure 4. The LD's frequency-intensity conversion coefficient k is 5×10^{-9} mW/Hz. Other parameters are the same as aforementioned. In Figure 4, the demodulation curve with $\Delta f_e = 0$ corresponds to the gyro system at its initial state without resonance frequency drift. But, in the practical situation the resonance frequency generally drifts from its initial value for even many FSRs due to the change of environmental factors, such as temperature. As can be seen in Figure 4, when the resonance frequency drifts from its initial value for $5FSR$ or $10FSR$, which corresponds to the curve with $\Delta f_e = 5FSR$ or $10FSR$, the slope of the demodulation curve is changed. That means the gyro system's scale factor actually varies with environmental factors. Nevertheless, in practice we use a fixed value for the scale factor, which is measured under a certain environment in advance, to convert the gyro's output values to rotation angular rate [34], which affects the measurement accuracy of the gyro system.

In order to analyse the characteristics of the scale factor under LD intensity modulation, the theoretically predicted scale factor K is calculated by Equation (9a). Figure 5 shows the relationship between the scale factor K and the resonance frequency drift, Δf_e . It can be found that the scale factor decreases as resonance frequency drift increases. For example, when the resonance frequency drifts for $10FSR$, the scale factor will be decreased from about -1.1×10^{-4} V/deg/s to -7.8×10^{-5} V/deg/s. This would induce measurement error for gyro system.

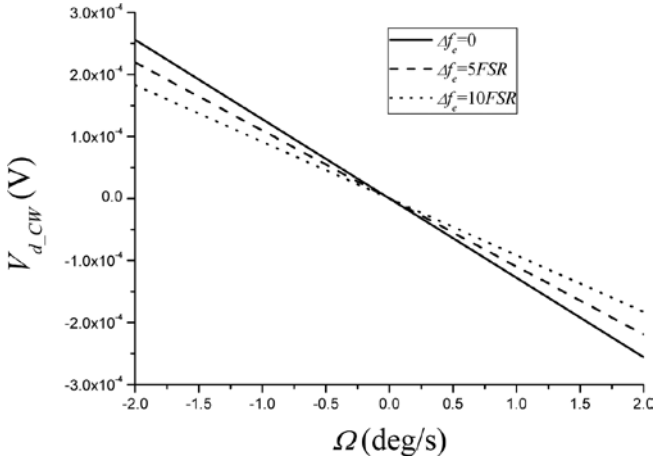


FIGURE 4 Demodulation curve with different values of Δf_e .

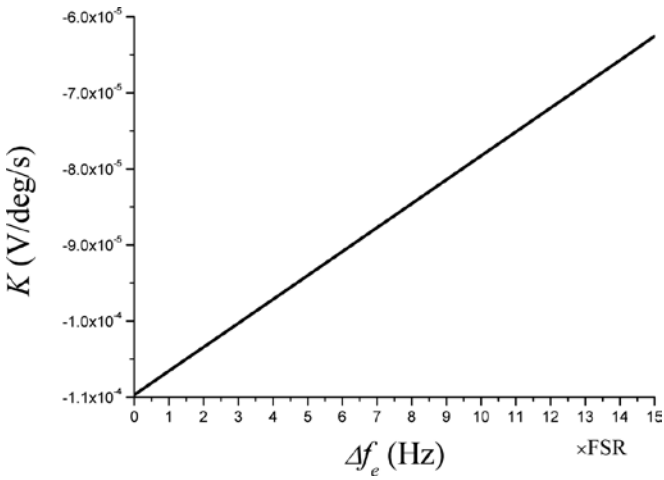


FIGURE 5 Graph showing the relationship between K and Δf_e .

According to Equations (7) to (9), the angular rate measurement error due to the scale factor drift could be expressed as

$$\Omega_e = \Omega_M - \Omega = \frac{V_{d_CW}(\Delta f_e, \Omega) - F_0}{K_0} - \Omega \quad (11)$$

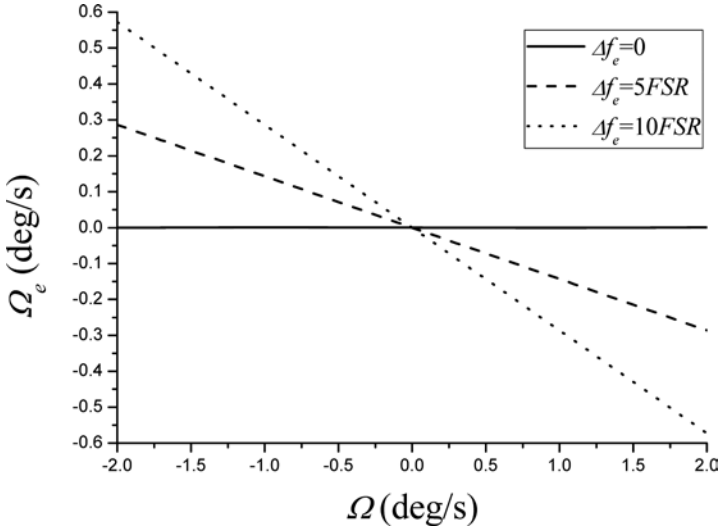


FIGURE 6
Relationship between Ω_e and Ω with different Δf_e .

where Ω_M is the measured value of input rotation angular rate, and K_0 and F_0 are respectively the scale factor and fitting zero offset when $\Delta f_e = 0$. Figure 6 shows the relationship between the angular rate measurement error Ω_e and the actual angular rate Ω with $\Delta f_e = 0, 5FSR$ and $10FSR$. The other parameters are the same as aforementioned. As can be seen from Figure 6, when the resonance frequency drift Δf_e is 0, the measurement error is very small that could not be obviously observed in Figure 6; however, the measurement error is largely increased as the resonance frequency drift increases to $5FSR$ or $10FSR$, which is because of the actual scale factor being changed from its initial value. In addition, it is found that a larger input angular rate corresponds to a larger measurement error. Taking the situation with $\Delta f_e = 5FSR$ as an example, the measurement error would be about -0.14 and -0.29 deg/s for input angular rate being 1.00 and 2.00 deg/s, respectively. This large error would seriously affect the accuracy of the gyro system.

4 CONCLUSIONS

The characteristics of an open-loop resonator fibre optic gyro (R-FOG) under laser diode (LD) accompanying intensity modulation caused by the dynamic input rotation angular rate and varied environmental factors induced resonance frequency drift has been looked into in detail. It is concluded that under the accompanying intensity modulation effect due to the dynamic input rotation angular rate, the linearity of the R-FOG system would be worsened

since the linear part of the demodulation curve trends to be bent and non-centrosymmetric, and simulation result shows that the scale factor nonlinearity of the gyro output increases as the LD's frequency-intensity conversion coefficient increases.

It is also found that the scale factor of the R-FOG system fluctuates under the resonance frequency drift induced accompanying intensity modulation. This scale factor fluctuation, which is found to increase as the resonance frequency drift or input rotation angular rate increases, would induce a system measurement error, and the numerical calculation result shows that the system measurement error would be as large as 0.29 deg/s with resonance frequency drift and input rotation angular rate being $5FSR$ and 2.00 deg/s, respectively, which should be counted for an open-loop R-FOG system.

These theoretical results are helpful to optimize and predict the performance of the R-FOG under intensity modulation. Besides, it is noted that when we design an R-FOG system employing an LD as the laser source, the injection current tuning induced intensity modulation effect should not be neglected, and adopting some appropriate methods, such as using a subtraction circuit [19-20], to eliminate this effect is necessary for realizing a high accuracy R-FOG.

ACKNOWLEDGMENT

The Project is Supported by Zhejiang Provincial Natural Science Foundation of China (LQ13F050001).

REFERENCES

- [1] Chow W.W., Gea-Banaciloche J., Pedrotti L.M., Sanders V.E., Schleich W. and Scully M.O. The ring laser gyro. *Reviews of Modern Physics* **57**(1) (1985), 61–103.
- [2] Shupe D.M. Fiber resonator gyroscope: Sensitivity and thermal nonreciprocity. *Applied Optics* **20**(2) (1981), 286–289.
- [3] Malvern A. Progress toward fiber optic gyro production. *Fiber Optic Gyros: 15th Anniversary Conference*. 1 February 1992, Boston, MA., USA. **1585**, pp. 48–64.
- [4] Meyer R.E., Ezekiel S., Stowe D.W. and Tekippe V.J. Passive fiber-optic ring resonator for rotation sensing. *Optics Letters* **8**(12) (1983), 644–646.
- [5] Ying D., Ma H. and Jin Z. Resonator fiber optic gyro using the triangle wave phase modulation technique. *Optics Communications* **281**(4) (2008), 580–586.
- [6] Iwatsuki K., Hotate K. and Higashiguchi M. Eigenstate of polarization in a fiber ring resonator and its effect in an optical passive ring-resonator gyro. *Applied Optics* **25**(15) (1986), 2606–2612.
- [7] Strandjord L.K. and Sanders G.A. Resonator fiber optic gyro employing a polarization-rotating resonator. *Fiber Optic Gyros: 15th Anniversary Conference*. 1 February 1992, Boston, MA., USA. **1585**, pp. 163–172.
- [8] Stocks L.F., Chodorow M. and Shaw H.J. All-single-mode fiber resonator. *Optics Letters* **7**(6) (1982), 288–290.

- [9] Jin Z., Yang Z., Ma H. and Ying D. Open-loop experiments in a resonator fiber-optic gyro using digital triangle wave phase modulation. *IEEE Photonics Technology Letters* **19**(20) (2007), 1685–1687.
- [10] Paoli T. L. and Ripper J. Direct modulation of semiconductor lasers. *Proceedings of the IEEE* **58**(10) (1970), 1457–1465.
- [11] Ma X., Li F. and Zhang M. Experimental study of polarization maintaining fiber ring resonator in fiber optic gyroscope. *Optical and Fiber Optic Sensor Systems*. 13 August 1998, Beijing, China. **3555**, pp. 363–367.
- [12] Takahashi M., Tai S. and Kyuma K. Effect of reflections on the drift characteristics of a fiber-optic passive ring-resonator gyroscope. *Journal of Lightwave Technology* **8**(5) (1990), 811–816.
- [13] Imai T., Nishide K.I., Ochi H. and Ohtsu M. Passive ring resonator fiber optic gyro using modulatable highly coherent laser diode module. *Fiber Optic Gyros: 15th Anniversary Conference*. 1 February 1992, Boston, MA., USA. **1585**, pp. 153–162.
- [14] Jin Z., Yu X. and Ma H. Resonator fiber optic gyro employing a semiconductor laser. *Applied Optics* **51**(15) (2012), 2856–2864.
- [15] Tatsuno K. and Tsunoda Y. Diode laser direct modulation heterodyne interferometer. *Applied Optics* **26**(1) (1987), 37–40.
- [16] Kobayashi S., Yamamoto Y., Ito M. and Kimura T. Direct frequency modulation in AlGaAs semiconductor lasers. *IEEE Journal of Quantum Electronics* **18**(4) (1982), 582–595.
- [17] Ma Y., Song P. and Wu X. Application research of external cavity semiconductor in resonant optical gyroscope. *Transducer and Microsystem Technologies* **30**(4) (2011), 51–56.
- [18] Ma Y. and Tang Y. Research on frequency tracking and locking for resonant optical gyro based on minimization of light source. *Transducer and Microsystem Technologies* **31**(1) (2012), 35–37.
- [19] Lei M., Feng L., Zhi Y., Liu H., Wang J., Ren X. and Su N. Current modulation technique used in resonator micro-optic gyro. *Applied Optics* **52**(2) (2013), 307–313.
- [20] Lei M., Feng L., Zhi Y., Liu H. and Su N. Experiments on resonator micro-optic gyro using external cavity laser diode. *Optical Engineering* **51**(10) (2012), 104602.
- [21] Hotate K. and Kikuchi Y. Analysis of thermo-optically induced bias drift in resonator fiber optic gyro. *Fiber Optic Sensor Technology II*. 1 March 2001, Boston, MA., USA. **4204**, pp. 81–88.
- [22] Ma H., Lu X., Yao L., Yu X. and Jin Z. Full investigation of the resonant frequency servo loop for resonator fiber-optic gyro. *Applied Optics* **51**(21) (2012), 5178–5185.
- [23] Ma H., Jin Z., Ding C. and Wang Y. Influence of spectral linewidth of laser on resonance characteristics in fiber ring resonator. *Chinese Journal of Lasers* **30**(8) (2003), 731–734.
- [24] Iwatsuki K., Hotate K. and Higashiguchi M. Kerr effect in an optical passive ring-resonator gyro. *Journal of Lightwave Technology* **4**(6) (1986), 645–651.
- [25] Zhang X., Ma H., Ding C. and Jin Z. Analysis on phase modulation spectroscopy of resonator fiber optic gyro. *Chinese Journal of Lasers* **32**(11) (2005), 1529–1533.
- [26] Jin Z., Zhang G., Mao H. and Ma H. Resonator micro optic gyro with double phase modulation technique using an FPGA-based digital processor. *Optics Communications* **285**(5) (2012), 645–649.
- [27] Iwatsuki K., Hotate K. and Higashiguchi M. Effect of Rayleigh backscattering in an optical passive ring-resonator gyro. *Applied Optics* **23**(21) (1984), 3916–3924.
- [28] Iwatsuki K., Hotate K. and Higashiguchi M. Backscattering in an optical passive-ring resonator gyro: experiment. *Applied Optics* **25**(23) (1986), 4448–4451.
- [29] Ma H., Jin Z., Ding C. and Wang Y. Research on Signal detection method of resonator fiber optical gyro. *Chinese Journal of Lasers* **31**(8) (2004), 1001–1005.
- [30] Carroll R., Coccoli C.D., Cardarelli D. and Coate G.T. The passive resonator fiber optic gyro and comparison to the interferometer fiber gyro. *Fiber Optic Gyros: 10th Anniversary Conference*. 11 March 1987, Cambridge, M.A., USA. **0719**, pp. 169–177.
- [31] Lefevre H. *The Fibre-Optic Gyroscope*. London: Artech House. 1993.

- [32] Wang X., Li A. and Xu H. Design of optical fiber gyroscope test system. *Modern Electronics Technique* **24** (2004), 46–48.
- [33] Hong L., Zhang C., Feng L. and Yu H. Investigation on scale factor and output nonlinearity in resonator micro-optic gyro. *Journal of Beijing University of Aeronautics and Astronautics* **38**(8) (2012), 1046–1050. (in Chinese)
- [34] Borenstein J. Experimental evaluation of a fibre optics gyroscope for improving dead-reckoning accuracy in mobile robots. *1998 IEEE International Conference on Robotics and Automation*. 16-20 May 1998, Leuven, Belgium. **4**, pp. 3456–3461.